

Anisotropic superconducting properties of $FeSe_{0.5}Te_{0.5}$ single crystals

Jia-Ming Zhao(赵佳铭) and Zhi-He Wang(王智河)

Citation: Chin. Phys. B, 2022, 31 (**9**): 097402. DOI: 10.1088/1674-1056/ac5610
Journal homepage: http://cpb.iphy.ac.cn; http://iopscience.iop.org/cpb

What follows is a list of articles you may be interested in

Josephson vortices and intrinsic Josephson junctions in the layered iron-based superconductor $Ca_{10}(Pt_3As_8)((Fe_{0.9}Pt_{0.1})_2As_2))_5$

Qiang-Tao Sui(随强涛), and Xiang-Gang Qui(邱祥冈)
Chin. Phys. B, 2022, 31 (**9**): 097403. DOI: 10.1088/1674-1056/ac76ae

Superconductivity at 44.4 K achieved by intercalating $EMIM^+$ into FeSe

Jinhua Wang(王晋花), Qing Li(李庆), Wei Xie(谢威), Guanyu Chen(陈冠宇), Xiyu Zhu(祝熙宇), and Hai-Hu Wen(闻海虎)
Chin. Phys. B, 2021, 30 (**10**): 107402. DOI: 10.1088/1674-1056/ac1f09

Superconducting anisotropy and vortex pinning in $CaKFe_4As_4$ and $KCa_2Fe_4As_4F_2$

A B Yu(于奥博), Z Huang(黄喆), C Zhang(张驰), Y F Wu(吴宇峰), T Wang(王腾), T Xie(谢涛), C Liu(刘畅), H Li(李浩), W Peng(彭炜), H Q Luo(罗会仟), G Mu(牟刚), H Xiao(肖宏), L X You(尤立星), and T Hu(胡涛)
Chin. Phys. B, 2021, 30 (**2**): 027401. DOI: 10.1088/1674-1056/abcf98

Anisotropy of $Ca_{0.73}La_{0.27}(Fe_{0.96}Co_{0.04})As_2$ studied by torque magnetometry

Ya-Lei Huang(黄亚磊), Run Yang(杨润), Pei-Gang Li(李培刚), Hong Xiao(肖宏)
Chin. Phys. B, 2020, 29 (**9**): 097405. DOI: 10.1088/1674-1056/ab9f26

Anomalous spectral weight transfer in the nematic state of iron-selenide superconductor

C Cai(蔡淙), T T Han(韩婷婷), Z G Wang(王政国), L Chen(陈磊), Y D Wang(王宇迪), Z M Xin(信子鸣), M W Ma(马明伟), Yuan Li(李源), Y Zhang(张焱)
Chin. Phys. B, 2020, 29 (**7**): 077401. DOI: 10.1088/1674-1056/ab90ec

---

Anisotropic superconducting properties of $FeSe_{0.5}Te_{0.5}$ single crystals

Jia-Ming Zhao(赵佳铭)[1] and Zhi-He Wang(王智河)[2,†]

[1] *School of Physics, Nanjing University, Nanjing* 210093, *China*
[2] *Center for Superconducting Physics and Materials, Collaborative Innovation Center of Advanced Microstructures and National Laboratory of Solid State Microstructures, Nanjing University, Nanjing* 210093, *China*

(Received 30 November 2021; revised manuscript received 21 January 2022; accepted manuscript online 17 February 2022)

We investigated the anisotropic electrical transport and magnetic properties of $FeSe_{0.5}Te_{0.5}$ single crystals grown by the self-flux method. The in-plane resistivity shows a metallic-like temperature dependence, while the out-of-plane resistivity shows a broad hump with a maximum at around 64 K. The magnetization loops for $H//c$-axis and $H//ab$-plane are also different, for example, there is a typical second peak for $H//c$-axis. The in-plane critical current density is larger than the out-of-plane one. The coherence length and penetration depth were estimated by the Ginzburg–Landau theory. The anisotropic parameter γ depends on the applied magnetic field and the temperature. The coupling of superconducting FeSe(Te) layers and the flux pinning mechanism relevant to anisotropy are also discussed.

Keywords: $FeSe_{1-x}Te_x$ single crystal, anisotropy, resistivity, magnetization

PACS: 74.25.–q, 74.25.F–, 74.25.Sv, 74.25.Wx **DOI:** 10.1088/1674-1056/ac5610

1. Introduction

The discovery of superconductivity at 8 K in FeSe with a PbO-type structure[1] has attracted great interest because of its simple crystal structure. The superconducting transition temperature T_c of FeSe has been enhanced to 14 K through the partial substitution of Te for Se,[2] to 38 K under high hydrostatic pressure[3] and to above 100 K in monolayer thin film.[4] In bulk $Fe_{1+y}Te_{1-x}Se_x$ crystals the optimal Te content to achieve the highest T_c is considered to be $x \approx 0.5$, and phase separation occurs in the region of $0.1 \leq x \leq 0.4$.[5] Although $Fe_{1+y}Te_{1-x}Se_x$ crystals have a layered structure, they have an anisotropy smaller than that of cuprate superconductors.[6,7] Mao *et al.* reported an anisotropy of 2.8 near T_c for $FeSe_{0.5}Te_{0.5}$,[8] close to the 2.6 reported by Yadav *et al.*[9] and 3.17 reported by Das *et al.*[10] For the applications of superconducting wires/tapes, the anisotropy of J_c, which also reflects its intrinsic crystallographic anisotropy, is an important parameter. The small superconducting anisotropy may facilitate fabrication of a dense superconducting wire/tape with a high critical current density. Therefore, detailed knowledge of the anisotropic properties of iron-based superconductors is important for potential applications.

It is believed that high-T_c superconductors, such as cuprates and iron-based superconductors, have distinct layered structures, the essence of which is the Josephson nature of the interlayer coupling. The values of the interlayer critical current J_c^c and the anisotropy γ can be used as a measure of the coupling strength and, as such, determine the three-dimensional electrodynamic and thermodynamic properties of these compounds. Generally, the anisotropy γ is a constant in the Ginzburg–Landau (G–L) model. However, it has been shown that the anisotropy γ depends on the temperature.[6,9] So far we have not found any signs of magnetic-field-related anisotropy. Our early work showed that the in-plane critical current density of $FeTe_{0.5}Se_{0.5}$ single crystal is higher than that of other single crystal compositions.[8] In this paper, we give detailed anisotropy parameters of $FeTe_{0.5}Se_{0.5}$ single crystal from measurements of electrical transport and magnetization, such as the upper critical field H_{c2}, the in-plane and out-of-plane critical current densities J_c^{ab} and J_c^c, respectively, the lower critical field H_{c1}, the coherence length ξ and the penetration depth λ. We give the field dependence of anisotropy γ at 13.5 K near T_c. The ratio of the in-plane and out-of-plane critical current densities increases with decreasing temperature, indicating that the coupling of the superconducting FeSe(Te) layer is suppressed. The flux pinning mechanism is also discussed.

2. Experimental method

The single crystals of $FeSe_{0.5}Te_{0.5}$ used in this experiment were grown by the self-flux method. Starting materials were powders of Fe (purity 3N), Se (purity 3N) and Te (purity 4N). The powders in the nominal composition were thoroughly mixed in an argon-filled glove box. The mixed powders were sealed in an evacuated quartz tube. The sealed quartz ampoule was placed in a furnace so that single crystals were grown from the bottom of an alumina crucible. The ampoule was heated at 650 °C for 24 h and then at 1110 °C for 72 h, then cooled down to 420 °C at a rate of 6 °C/h and kept there for 70 h, followed by quenching in water. The as-grown single crystal with a shiny flat surface is easily

†Corresponding author. E-mail: zhwang@nju.edu.cn

© 2022 Chinese Physical Society and IOP Publishing Ltd

cleaved. Recently, Uhrig *et al.*[11] reported the effect of annealing $FeSe_{0.35}Te_{0.65}$ single crystals in different atmospheres on the surface chemistry, the superconducting transition temperature T_c and the critical current density J_c. Their experimental results indicate that the improvement in the superconducting properties is strongly correlated with the formation of a thin iron oxide surface layer. To avoid possible oxidation of the surface layer and uncertain consequences for the intrinsic superconducting properties, we chose unannealed $FeSe_{0.5}Te_{0.5}$ single crystal to study its anisotropy.

The x-ray diffraction (XRD) pattern of $FeSe_{0.5}Te_{0.5}$ single crystal was detected by a standard Cu-anode powder diffractometer (Siemens D5000) at room temperature. The electric transport measurements were performed on a commercial physical properties measurement system (PPMS-9 T, Quantum Design) using a standard four-probe configuration. Gold wires of diameter 0.05 mm were pasted on the sample surface with silver paste. To obtain the resistivity along the *c*-axis, we used symmetrical current and voltage electrodes on the top and bottom surfaces using indium metal to decrease the contact resistance. The area of the current electrode was larger than that of the voltage electrode to keep the current along the *c*-axis. The magnetization measurements were also carried out on the PPMS with a vibrating sample magnetometer (VSM). The magnetic field was applied along the *c*-axis and/or the *ab*-plane. The sample sizes used in transport measurements for $I//ab$-plane and $I//c$-axis and magnetization measurements for $H//c$-axis and $H//ab$-plane were about 2.8 mm × 2 mm × 0.4 mm and 2 mm × 1.4 mm × 0.4 mm, respectively. The smaller sample was cut from the larger size single crystal.

3. Results and discussion

Figure 1 shows the XRD pattern of $FeSe_{0.5}Te_{0.5}$ single crystal tested at room temperature. Compared with the standard card, we see tetragonal symmetry $P4/nmm$ for the main $FeSe_{0.5}Te_{0.5}$ phase and hexagonal symmetry $P63/mmc$ for the impurity phase Fe_7Se_8. This impurity also appears in other papers.[12,13] What is more, the appearance of the (104) peak may come from the twin boundaries.[14,15] The strong (00*l*) peaks indicate that the *c*-axis of the crystal is perpendicular to the cleaved surface. The lattice parameters obtained from different peaks were averaged by the Bragg formula, for example, $c = 0.60165$ nm, which agrees with the data from previous papers.[16–18]

The temperature dependence of in-plane (squares) and out-of-plane (circles) resistivity is measured from 300 K to 10 K at zero field, as shown in the inset of Fig. 2(a). Superconductivity occurs near 14 K. The in-plane resistivity shows a metallic-like temperature dependence, while the out-of-plane resistivity shows a broad hump with maximum at around 64 K.

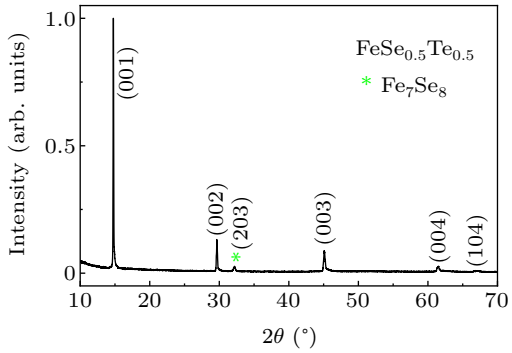


Fig. 1. XRD pattern for $FeSe_{0.5}Te_{0.5}$ single crystals.

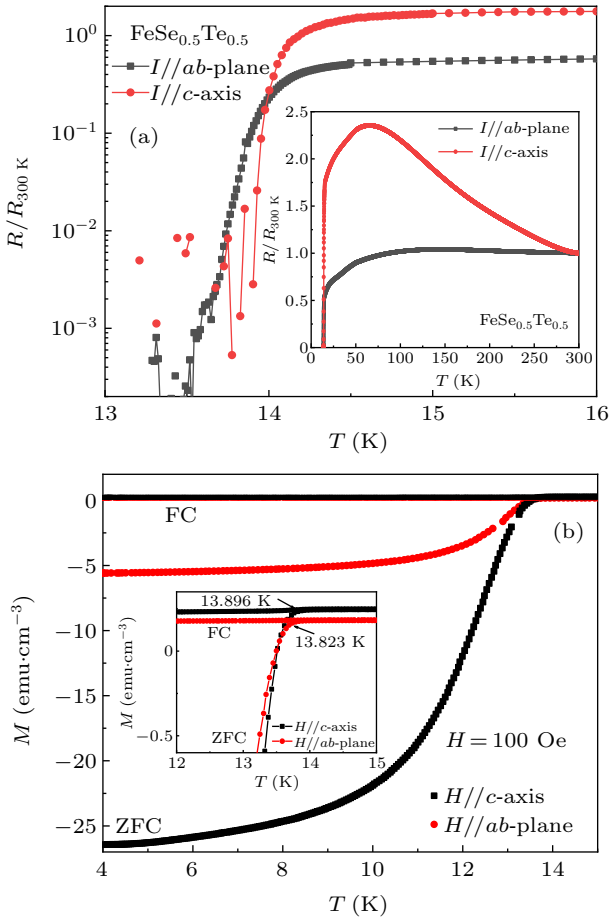


Fig. 2. (a) Temperature dependence of reduced resistance near T_c for $I//ab$-plane and $I//c$-axis. The inset is for temperature from 300 K to 10 K. (b) Temperature dependence of magnetic susceptibility from 15 K to 4 K at 0.01 T for $H//c$-axis and $H//ab$-plane. The inset shows enlarged plots in the vicinity of T_c.

A similar result was reported by Noji *et al.*[19] A broad hump is also observed in the in-plane resistivity in materials such as $K_xFe_2Se_2$, $Cs_xFe_2Se_2$, and $Rb_xFe_{2-y}Se_2$.[20–22] Generally, the broad maximum of in-plane resistivity is thought to arise from the scattering potential of randomly distributed Fe ions in the Fe plane, whereas the broad maximum of out-of-plane resistivity may be ascribed to the *c*-axis energy gap of the interlayer structure. In order to see clearly both the superconducting transition T_c^{ab} for $I//ab$-plane and T_c^{c} for $I//c$-axis, we show the enlarged main plot in Fig. 2(a). It shows that the out-of-plane T_c^{c} is higher than the in-plane T_c^{ab}, which, however,

is not consistent with the following magnetization result. Figure 2(b) shows the zero-field cooled and field-cooled curves measured at 0.01 T for $H//ab$-plane and $H//c$-axis, respectively. The critical temperature for $H//c$-axis corresponds to the in-plane critical temperature T_c^{ab} and that for $H//ab$-plane to the out-of-plane T_c^c. The enlarged $M(T)$ result, shown in the inset of Fig. 2(b), displays $T_c^{ab} = 13.896$ K, higher than $T_c^c = 13.823$ K. The discrepancy in T_c from transport and magnetic measurements may be caused by the measured current density and the heat effect of contact resistance in Fig. 2(a). In addition, the sample's magnetic susceptibility for $H//c$-axis is about five times greater than that for $H//ab$-plane at 4 K. This result indicates an anisotropic critical current density, namely, $J_c^{ab} \neq J_c^c$. From Fig. 2(b), we can obtain $\chi = -3.32$ at 4 K. Thus, the superconducting volume fraction of the unannealed $FeSe_{0.5}Te_{0.5}$ single crystal should be close to 100%.

The angular dependences of in-plane resistance R_{ab} and out-of-plane resistance R_c measured at 13.5 K for several fixed fields H_0 up to 9 T are shown in the inset of Figs. 3(a) and 3(b), respectively. All $R(\theta)$ curves show a periodic change. The resistance is maximum at 0° and/or 180° ($H//c$-axis) and minimum at 90° ($H//ab$-plane), indicating there is a field-induced anisotropy of resistance. In addition R_c is smaller than 1 mΩ and the signal of thermal fluctuation, especially at large angles, is not negligible and results in an unsmooth curve, as seen in inset of Fig. 3(b). Based on the anisotropic G–L theory, an anisotropic material can be transformed into an isotropic material by means of a scaling approach[23] in the following form:

$$H_{\rm eff}^{//c}(\theta) = H_0\sqrt{\cos^2(\theta) + \gamma^{-2}\sin^2(\theta)}, \tag{1}$$

where γ is the anisotropy parameter of the single crystal and θ is the angle between the applied magnetic field and the c-axis of the crystal. However, the scaling approach is based on a simple rescaling of the coordinate axes (i.e., $x = x'$, $y = y'$, $\gamma z = z'$), which is incomplete for a complex system. Therefore, in order to have a reference curve for scaling, we measured the field dependence of resistance at 13.5 K for $H//c$-axis (empty squares in Fig. 3(a) for $I//ab$-plane and Fig. 3(b) for $I//c$-axis). For the best value of the anisotropic parameter, $R(\theta)$ curves (or $R(H_{\rm eff})$) were fitted to the experimental $R(H)$ to ensure the best possible agreement in a range of angles starting from zero. The best fitting results are plotted in Fig. 3(a) for in-plane resistance and in Fig. 3(b) for out-of-plane resistance. From Figs. 3(a) and 3(b), it is no surprise to see that the best fit lies near 0° and/or 180° ($H//c$-axis) and meanwhile the biggest deviation from $R(H)$ is at angles approaching the ab-plane. The deviant angle appears with increasing applied field, meanwhile the anisotropy parameter γ_H decreases with it. The field dependence of the anisotropy parameter γ_H is shown in Fig. 3(c). As seen in the inset of Fig. 3(c), the two γ_H curves agree reasonably well with each other and both show a power law behavior,

$$\gamma_H \propto H^{-\alpha}, \tag{2}$$

where $\alpha = 0.76$ for $I//ab$-plane and $\alpha = 0.64$ for $I//c$-axis. This result shows that the anisotropy parameter γ in G–L theory is not a constant and depends on the applied magnetic field and the temperature.

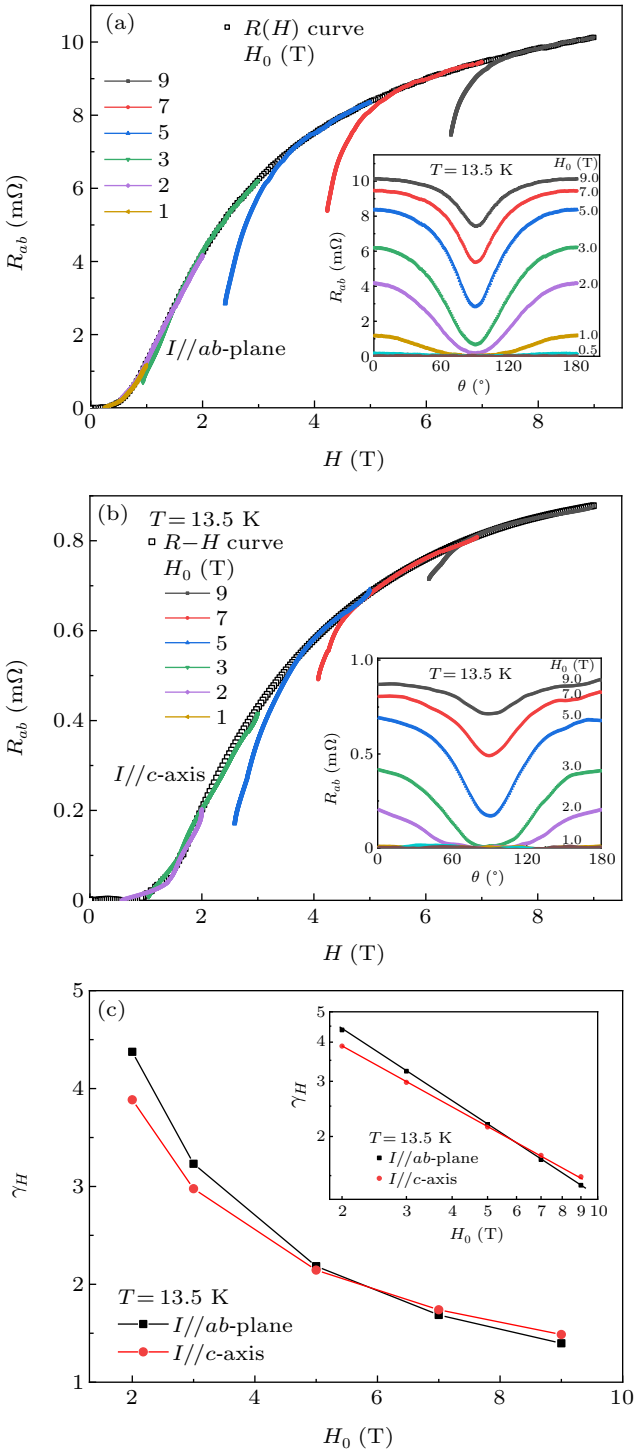


Fig. 3. (a) Field dependence of resistance at 13.5 K (a) for $I//ab$-plane and (b) $I//c$-axis, and the scaled result of $R(\theta)$ in the inset. (c) Field dependence of anisotropic parameter for both $I//ab$-plane and $I//c$-axis with a double logarithmic plot.

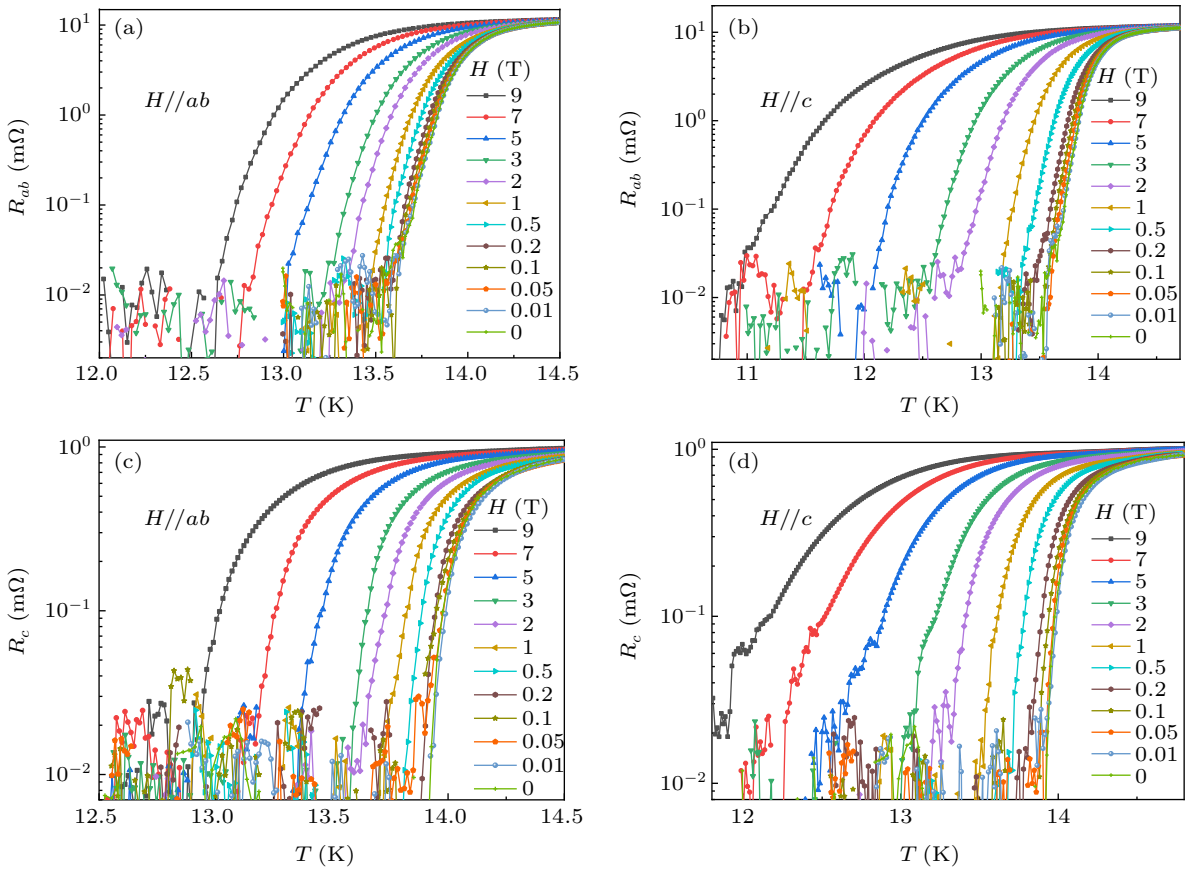


Fig. 4. Temperature dependence of resistance in the vicinity of T_c at several fixed fields: (a) $I//ab$, $H//ab$; (b) $I//ab$, $H//c$; (c) $I//c$, $H//ab$; (d) $I//c$, $H//c$.

Figure 4 gives the temperature dependence of in-plane and out-of-plane resistivity measured at several fixed applied magnetic fields up to 9 T for $H//ab$-plane and $H//c$-axis, respectively. With increasing field, the low-resistance part of the $R(T)$ curve gets broader towards low temperatures. The field-induced broadening for $H//c$ is larger than that for $H//ab$, indicating that the single crystal has an anisotropic upper critical field. If we define the temperature where the resistance is 10% of the normal state resistance R_n as the critical temperature T_c, the temperature dependence of the upper critical field $H_{c2}(T)$ can be obtained as shown in Fig. 5(a). All $H_{c2}(T)$ curves are upward, indicating that they should follow the expression

$$H_{c2} = H_{c2,0}\left(1 - \frac{T_c}{T_{c0}}\right)^n. \tag{3}$$

The relationship between H_{c2} and $1-(T_c/T_{c0})$ is plotted in the inset of Fig. 5(a) and it is linear with different n. For current parallel to the ab plane, n is 1.23 for $H//c$-axis and 1.30 for $H//ab$-plane; while for current parallel to the c-axis, n is 1.36 and 1.25, respectively. From the $H_{c2}(T)$ expression we can get the temperature dependence of the anisotropic upper critical field parameter $\gamma_{H_{c2}} = H_{c2}^{ab}/H_{c2}^{c}$ as shown in Fig. 5(b). $\gamma_{H_{c2}}$ increases slightly with decreased temperature, and the anisotropy $\gamma_{H_{c2}}$ for $I//ab$-plane is bigger than that for $I//c$-axis. This result implies that the anisotropy $\gamma_{H_{c2}}$ relates to the direction of the applied current and the effective flux pinning energy. The electric field along the c-axis may promote the coupling of electrons between superconducting layers and weaken the anisotropy of the sample.

It is well known that the $R(T)$ curve in applied fields near T_c contains the dynamics of magnetic flux motion. In thermally activated flux flow models, the resistivity below 1% ρ_n can be described by the Arrhenius relation[24]

$$\rho = \rho_0 \exp\left(-\frac{U}{k_B T}\right), \tag{4}$$

where U is the thermally activated energy or effective pinning energy. From Fig. 4, the effective pinning energy can be extracted from the in-plane $R(T)$ data. We transfer the R–T curve into a $\ln\rho$–$1/T$ plot. The slope of the $\ln\rho$–$1/T$ curve is the effective pinning energy U. The field dependence of the effective pinning energy $U(H)$ is depicted in Fig. 5(c). The U values for $H//ab$ are much higher than those for $H//c$, indicating that an intrinsic-like flux pinning originating from the layered structure plays an important role in the single crystal. This result is often reported for high-T_c superconductors[25,26] and iron-based superconductors.[27,28] The field dependence of the effective pinning energy $U(H)$ follows

$$U \propto H^{-\beta} \tag{5}$$

with a crossover at about 2 T. In low-field region, the β value is 0.17 for $H//c$-axis and 0.09 for $H//ab$-plane. In the higher-field region, the β value is 0.28 for $H//c$-axis and 0.29 for $H//ab$-plane. For the low-field region flux pinning is considered to be dominated by a single magnetic flux line, while for the higher field region collective flux pinning plays an important role.[27] $\beta \approx 0.3$ implies that the flux lines are collectively pinned by the planar dislocations and columnar defects.[8] In addition, we take the ratio γ_U of U_{ab} to U_c as the anisotropy parameter of effective pinning energy, as shown in the inset of Fig. 5(c). γ_U increases quickly for $H < 2$ T and then becomes constant for $H > 2$ T. This result may support the crossover from single flux pinning to collective flux pinning in the crystal.

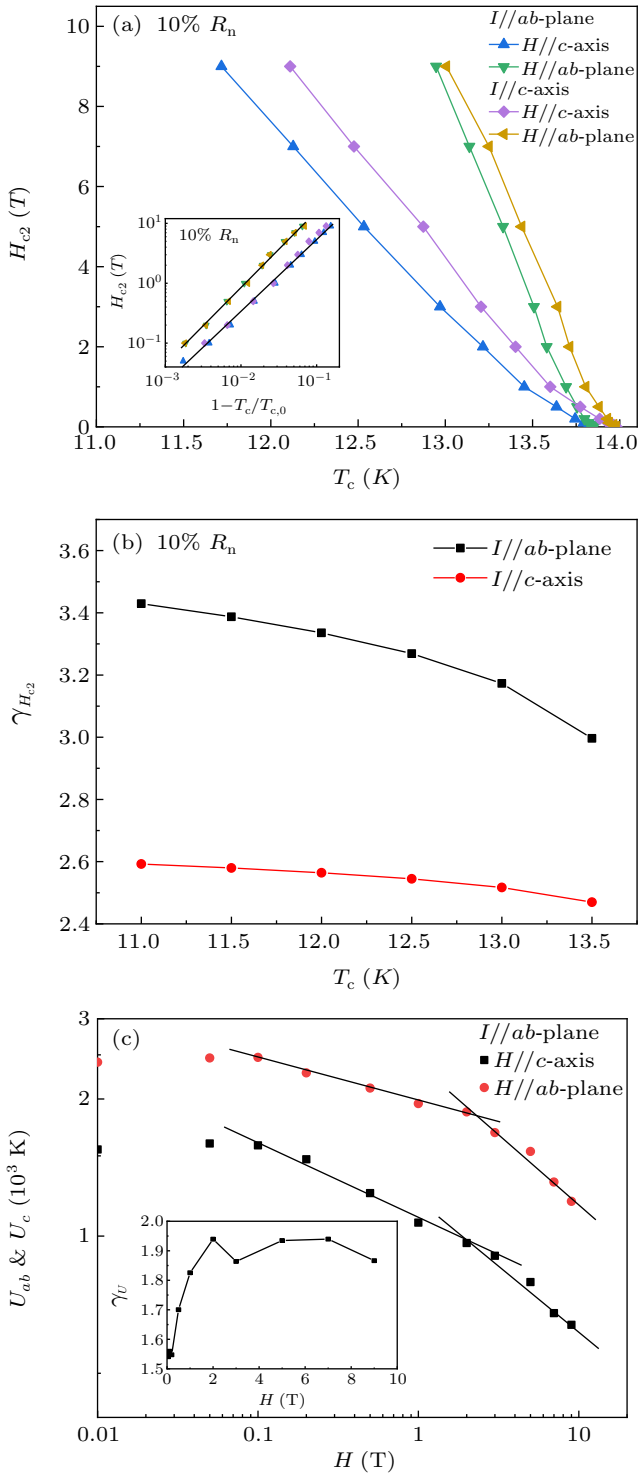


Fig. 5. (a) Field dependence of the upper critical field $H_{c2}(T)$ determined by certain criteria of $R = 10\%R_n$. The inset is a log–log logarithmic plot. (b) Temperature dependence of H_{c2}^{ab}/H_{c2}^{c} for $I//ab$-plane and $I//c$-axis. (c) Field dependence of the effective pinning energy with $I//ab$-plane for $H//ab$-plane and $H//c$-axis. The inset is the field dependence of the anisotropic effective pinning energy.

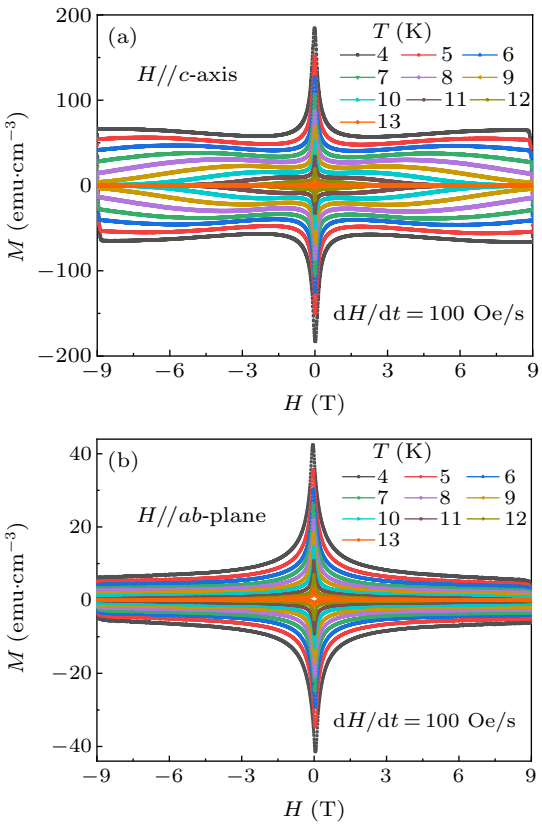


Fig. 6. Isothermal magnetization loops at several temperatures from 4 K to 13 K at intervals of 1 K and a sweep rate of 100 Oe·s^{-1}: (a) $H//c$-axis, (b) $H//ab$-plane.

Figure 6 shows the isothermal magnetization loops measured at several temperatures from 4 K to 13 K in intervals of 1 K for $H//c$-axis and $H//ab$-plane. In order to avoid the influence of the residual magnetic moment, the isothermal magnetization loop from −9 T to 9 T at 14 K is measured as a background magnetization and deducted from the other loops. The isothermal magnetization loops for $H//c$-axis is different from that for $H//ab$-plane. The $M(H)$ curve for $H//c$-axis has a significant peak, and the peak moves towards a low field as the temperature increases. The peak disappears near T_c. A similar peak effect also exists in $FeSe_{0.5}Te_{0.5}$ single crystal,[10] $YBa_2Cu_3O_{7-\delta}$ single crystal[29] and $Ba_{0.6}K_{0.4}Fe_2As_2$.[30] The peak effect is considered to be related to the transition from an elastic to a plastic deformation regime in the vortex lattice, in which the strong pinning centers exist from correlated disorder such as twin boundaries, planar dislocations and/or columnar defects.[14] However, for $H//ab$-plane, none of the isothermal

magnetization loops show a peak effect. Das *et al.*[10] also reported a similar behavior. The magnetization produced by the loop consists of in-plane superconducting current density J_c^{ab} and out-of-plane J_c^c. J_c^c depends on the coupling and pinning centers of superconducting FeSe(Te) layers and is smaller than J_c^{ab}. The weak pinning forces between superconducting FeSe(Te) layers result in a monotonic decrease with increasing applied field.

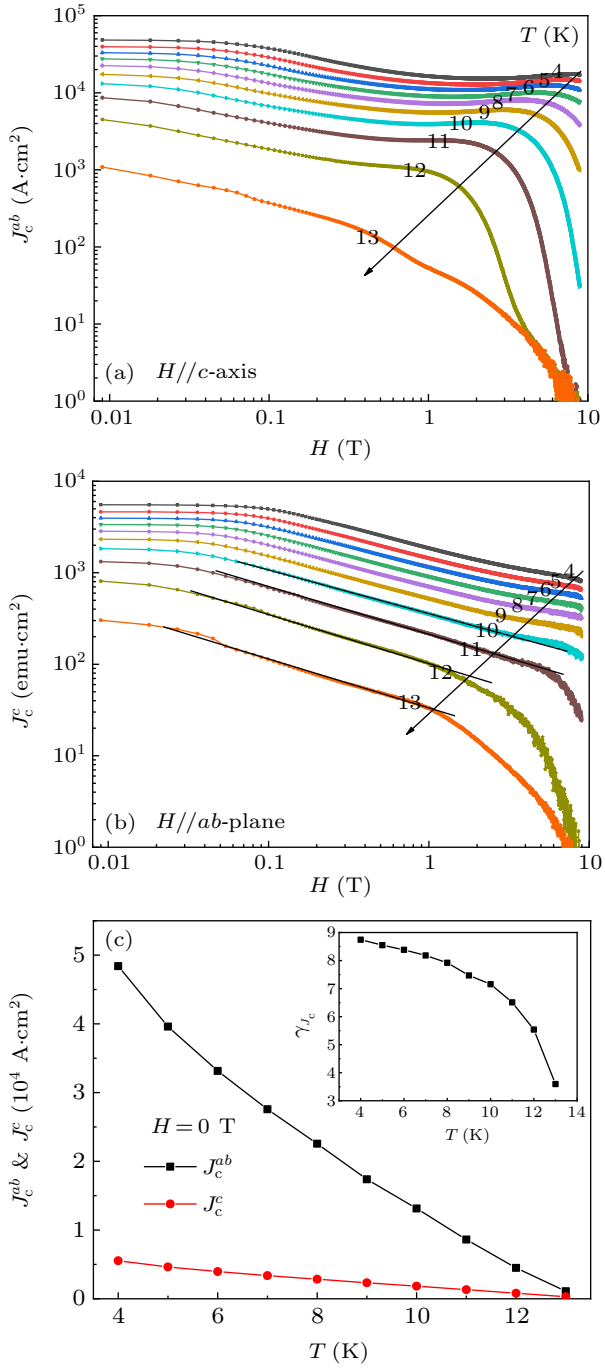


Fig. 7. [(a), (b)] The field dependence of critical current density J_c^{ab} and J_c^c, respectively, at several temperatures from 4 K to 13 K. (c) Temperature dependence of critical current density at 0 T for J_c^{ab} and J_c^c. The inset shows the temperature dependence of anisotropic critical current density.

According to the Bean critical state model,[31] the field dependence of critical current density $J_c(H)$ can be obtained from the following equations:

$$J_c^{ab} = \frac{20\Delta M}{a\left(1-\frac{a}{3b}\right)}, \quad H//c, \tag{6}$$

$$J_c^c = \frac{20\Delta M}{b}, \quad H//ab, \tag{7}$$

where $\Delta M = M(B_-) - M(B_+)$, $M(B_-)$ and $M(B_+)$ are the magnetizations when sweeping fields down and up, respectively, and a, b are the sample surface widths (in cm) with $a < b$.[32] The measured M is in emu·cm^{-3} and J_c is in A·cm^{-2}. Values of $J_c(H)$ at several fixed temperatures are reported in Fig. 7(a) for $H//c$-axis and in Fig. 7(b) for $H//ab$-plane. From Fig. 7(a), the critical current density at higher-field regions is enhanced and cannot be given by a simple expression. But for Fig. 7(b), the field dependence of the critical current density $J_c(H)$ follows a power-law behavior, $J_c \propto H^{-p}$ with $p \sim 0.53$. In addition, by taking the value of $J_c(H=0)$ at different temperatures, the temperature dependence of $J_c^{ab}(T)$ and $J_c^c(T)$ is shown in Fig. 7(c). The values of J_c^{ab} and J_c^c increase with decreasing temperature. If we define the anisotropy of the critical current density $\gamma_{J_c} = J_c^{ab}(T)/J_c^c(T)$, γ_{J_c} is not a constant and increases with decreasing temperature, as shown in the inset of Fig. 7(c). This result implies that the coupling between the superconducting FeSe(Te) layers is suppressed by the temperature and results in an increase in the anisotropy of the critical current density.

To obtain the temperature dependence of the lower critical field H_{c1} we measured the zero-field cooled $M(H)$ curves with a low sweeping field rate of 10 Oe·s^{-1} at several fixed temperatures for $H//c$-axis and $H//ab$-plane. Figure 8(a) shows the data for $H//c$-axis. In general, the lower critical field H_{c1} was extracted from the deviation of the $M(H)$ curve from linear in the low-field region. However, the diamagnetic signal of the sample does not always increase linearly with strengthening magnetic field in Fig. 8(a), especially at higher temperatures, due to flux penetration and pinning. So, the diamagnetic signal quickly deviates from linearity but still continues to strengthen as the magnetic field intensifies and a dip in the $M(H)$ curves appears as the diamagnetism reaches a maximum. After that, the flux lines enter the sample, resulting in the suppression of magnetization. Here, we define the dip field H_{dip} as the lower critical field H_{c1}, and obtain the temperature dependence of the lower critical field H_{c1} for $H//c$-axis and $H//ab$-plane, as shown in Fig. 8(b). H_{dip}^{ab} for $H//ab$ is larger than H_{dip}^c for $H//c$, indicating that it is more difficult for the magnetic flux to penetrate into the sample for $H//ab$. This result also shows the response of a layered structure to anisotropic flux pinning. Therefore H_{dip} also shows obvious anisotropy, as shown in the inset of Fig. 8(b), and $\gamma_{H_{dip}}$ decreases with decreasing temperature. It obeys the following expression:

$$H_{dip} = H_{dip,0}\left(1-\frac{T_c}{T_{c0}}\right)^m, \tag{8}$$

where m is 1.23 for $H//c$-axis and 1.11 for $H//ab$-plane.

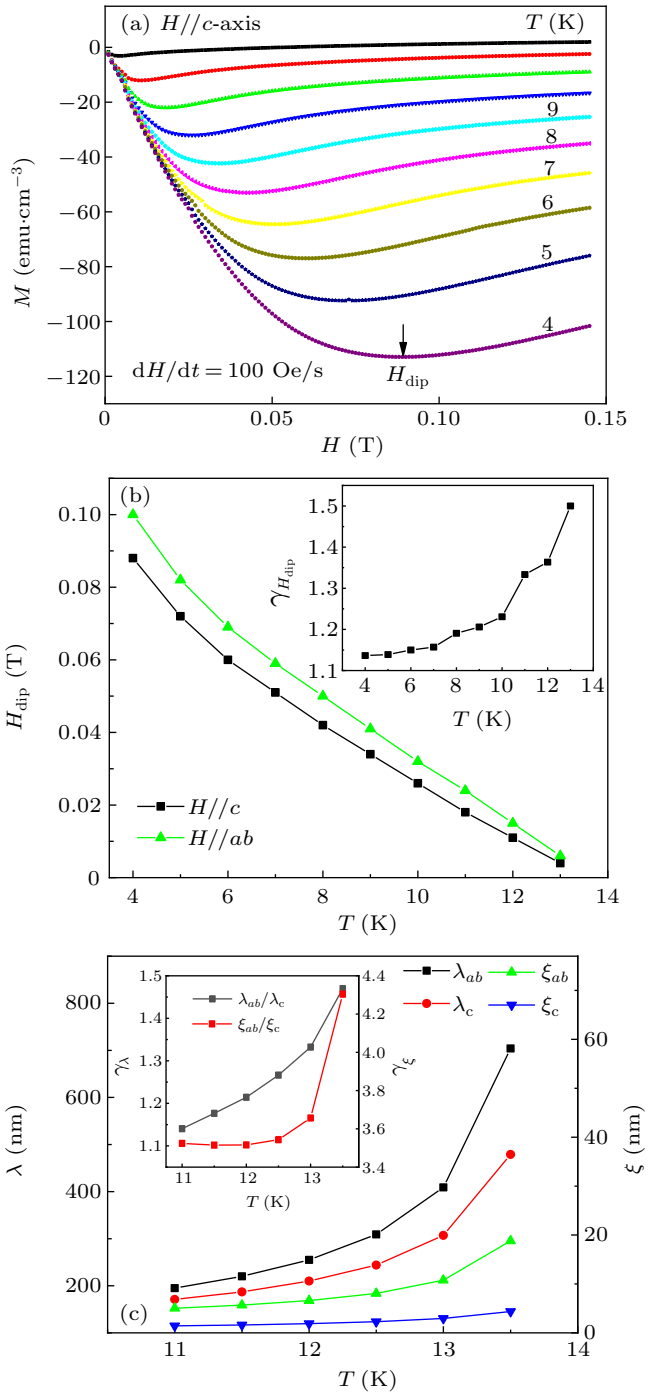


Fig. 8. (a) Field dependence of magnetic moments at a sweep rate of 10 Oe·s^{-1}. (b) Temperature dependence of the dip field for $H//c$-axis and $H//ab$-plane. The inset shows the temperature dependence of the anisotropic dip field. (c) The magnetic penetration depth and coherence length resulting from (b) and Fig. 5(a). The inset shows the temperature dependence of the anisotropic parameter of penetration depth and coherence length.

The magnetic penetration depth λ and coherence length ξ are important parameters for superconductors. They are estimated from the following basic relations:[33]

$$H_{c2}^{c} = \frac{\Phi_0}{2\pi\xi_{ab}^2}, \text{ for } H//c, \tag{9}$$

$$H_{c2}^{ab} = \frac{\Phi_0}{2\pi\xi_{ab}\xi_c}, \text{ for } H//ab, \tag{10}$$

$$H_{c1}^{c} = \frac{\Phi_0}{8\pi\mu_0\lambda_{ab}^2}\left[2\ln\left(\frac{\lambda_{ab}}{\xi_{ab}}\right)+1\right], \text{ for } H//c, \tag{11}$$

$$H_{c1}^{ab} = \frac{\Phi_0}{8\pi\mu_0\lambda_{ab}\lambda_c}\left[\ln\left(\frac{\lambda_{ab}\lambda_c}{\xi_{ab}\xi_c}\right)+1\right], \text{ for } H//ab. \tag{12}$$

For the $FeSe_{0.5}Te_{0.5}$ single crystal, the temperature dependences of the magnetic penetration depth (λ_{ab} and λ_c) and the coherence length (ξ_{ab} and ξ_c) are obtained from the H_{c2}^{ab}, H_{c2}^{c}, H_{c1}^{ab}, and H_{c1}^{c} shown in Figs. 5(a) and 8(b), and given in Fig. 8(c). From Fig. 8(c), λ_{ab} is larger than λ_c. This result shows that the flux lines for $H//c$-axis enter more easily into the sample than those for $H//ab$-plane. This is consistent with our above result originating from the layered structure. Meanwhile, ξ_{ab} is larger than ξ_c, indicating that the coupling of superconducting electrons in the ab-plane is stronger than along the c-axis. This is consistent with the anisotropic critical current density. Extrapolating to $T = 0$ K, we have $\lambda_{ab} = 74$ nm, $\xi_{ab}(0) = 1.9$ nm, $\lambda_c = 78$ nm and $\xi_c(0) = 0.64$ nm. The extrapolated coherence length $\xi_{ab}(0)$ is close to that reported in the literature,[34] but the penetration depth is an order of magnitude smaller than previously reported,[6] which is ascribed to our larger dip field H_{dip} than H_{c1} that deviates from the linear $M(H)$. Furthermore, the anisotropy of penetration depth and coherence length, γ_λ and γ_ξ, is shown in the inset of Fig. 8(c). They decrease monotonously with decreasing temperature.

4. Conclusion

By combining measurements of electric transport for $I//ab$-plane and $I//c$-axis and magnetization for $H//c$-axis and $H//ab$-plane we obtain detailed anisotropic superconducting properties of $FeSe_{0.5}Te_{0.5}$ single crystal. The in-plane resistivity shows a metallic-like temperature dependence, while the out-of-plane resistivity shows a broad hump with a maximum at around 64 K. The scaling of $R(\theta)$ gives a field-induced anisotropic parameter. The electric transport measurements imply that the anisotropy of the upper critical field $\gamma_{H_{c2}}$ may relate to the direction of the applied current and the effective flux pinning energy. The magnetization measurement shows an anisotropic critical current density. Decreasing temperature can enhance the critical current density and suppress the coupling between the superconducting FeSe(Te) layers. The coherence length and penetration depth estimated by the GL theory are consistent with the electric transport and magnetization data. The anisotropic superconducting properties are related to its layered structure.

Acknowledgments

The authors acknowledge National Laboratory for Solid State Microstructures and Center for Superconductivity Physics and Materials, Nanjing University for sample preparation and physical property measurements.

Project supported by the National Key Research and Development Program of China (Grant No. 2016YFA0300401) and the Strategic Priority Research Program of Chinese Academy of Sciences (Grant No. XDB25000000).

References

[1] Hsu F C, Luo J Y, Yeh K W, Chen T K, Huang T W, Wu P M, Lee Y C, Huang Y L, Chu Y Y, Yan D C and Wu M K 2008 *Proc. Natl. Acad. Sci. USA* **105** 14262

[2] Sales B C, Sefat A S, McGuire M A, Jin R Y, Mandrus D and Mozharivskyj Y 2009 *Phys. Rev. B* **79** 094521

[3] Sun J P, Matsuura K, Ye G Z, Mizukami Y, Shimozawa M, Matsubayashi K, Yamashita M, Watashige T, Kasahara S, Matsuda Y, Yan J Q, Sales B C, Uwatoko Y, Cheng J G and Shibauchi T 2016 *Nat. Commun.* **7** 12146

[4] Ge J F, Liu Z L, Liu C, Gao C L, Qian D, Xue Q K, Liu Y and Jia J F 2015 *Nat. Mater.* **14** 285

[5] Fang M H, Pham H M, Qian B, Liu T J, Vehstedt E K, Liu Y, Spinu L and Mao Z Q 2008 *Phys. Rev. B* **78** 224503

[6] Bendele M, Weyeneth S, Puzniak R, Maisuradze A, Pomjakushina E, Conder K, Pomjakushin V, Luetkens H, Katrych S, Wisniewski A, Khasanov R and Keller H 2010 *Phys. Rev. B* **81** 224520

[7] Larbalestier D, Gurevich A, Feldmann D M and Polyanskii A 2001 *Nature* **414** 368

[8] Mao R, Wu Z, Wang Z, Pan Z, Xu M and Wang Z 2019 *J. Alloys Compd.* **809** 151851

[9] Yadav A K, Kushwaha V K and Tomy C V 2015 *AIP. Conf. Proc.* **1665** 130023

[10] Das P, Thakur A D, Yadav A K, Tomy C V, Lees M R, Balakrishnan G, Ramakrishnan S and Grover A K 2011 *Phys. Rev. B* **84** 214526

[11] Uhrig D M, Williams G V M, Bioletti G and Chong S V 2020 *Supercond. Sci. Technol.* **33** 055006

[12] Tsurkan V, Deisenhofer J, Günther A, Kant C, Klemm M, Krug von Nidda H A, Schrettle F and Loidl A 2011 *The European Physical Journal B* **79** 289

[13] Taen T, Tsuchiya Y, Nakajima Y and Tamegai T 2009 *Phys. Rev. B* **80** 092502

[14] Galluzzi A, Buchkov K, Tomov V, Nazarova E, Leo A, Grimaldi G, Nigro A, Pace S and Polichetti M 2018 *Supercond. Sci. Technol.* **31** 015014

[15] Liang C, Zhang J, Zhao K, Yang X S and Zhao Y 2020 *Acta Phys. Sin.* **69** 237401 (in Chinese)

[16] Yeh K W, Huang T W, Huang Y L, Chen T K, Hsu F C, Wu P M, Lee Y C, Chu Y Y, Chen C L, Luo J Y, Yan D C and Wu M K 2008 *Europhys. Lett.* **84** 37002

[17] Imai Y, Sawada Y, Nabeshima F and Maeda A 2015 *Proc. Natl. Acad. Sci. USA* **112** 1937

[18] Wu Z F, Tao J, Xu X B, Qiu L, Yang S G and Wang Z H 2016 *Phys. C* **528** 39

[19] Noji T, Suzuki T, Abe H, Adachi T, Kato M and Koike Y 2010 *J. Phys. Soc. Jpn.* **79** 084711

[20] Ying J J, Wang X F, Luo X G, Li Z Y, Yan Y J, Zhang M, Wang A F, Cheng P, Ye G J, Xiang Z J, Liu R H and Chen X H 2011 *New J. Phys.* **13** 033008

[21] Wang A F, Ying J J, Yan Y J, Liu R H, Luo X G, Li Z Y, Wang X F, Zhang M, Ye G J, Cheng P, Xiang Z J and Chen X H 2011 *Phys. Rev. B* **83** 060512

[22] Guo J, Jin S, Wang G, Wang S, Zhu K, Zhou T, He M and Chen X 2010 *Phys. Rev. B* **82** 180520

[23] Blatter G, Geshkenbein V B and Larkin A I 1992 *Phys. Rev. Lett.* **68** 875

[24] Blatter G, Feigel'man M V, Geshkenbein V B, Larkin A I and Vinokur V M 1994 *Rev. Mod. Phys.* **66** 1125

[25] Palstra T T, Batlogg B, Schneemeyer L F and Waszczak J V 1988 *Phys. Rev. Lett.* **61** 1662

[26] Wang Z H and Cao X W 1999 *Solid. State. Commun.* **109** 709

[27] Lin H, Dong C, Pan X, Yao C, Zhang X, Zhao Y and Ma Y 2020 *Supercond. Sci. Technol.* **33** 125001

[28] Lei H, Hu R, Choi E S and Petrovic C 2010 *Phys. Rev. B* **82** 134525

[29] Erb A, Genoud J Y, Marti F, Dumling M, Walker E and Flkiger R 1996 *J. Low. Temp. Phys.* **105** 1023

[30] Yang H, Luo H, Wang Z and Wen H H 2008 *Appl. Phys. Lett.* **93** 142506

[31] Bean C P 1964 *Rev. Mod. Phys.* **36** 31

[32] Wiesinger H P, Sauerzopf F M and Weber H W 1992 *Phys. C* **203** 121

[33] Tinkham M 2004 *Introduction to Superconductivity* (2nd edn.) (New York: Dover Publication) pp. 134–135, 149–154

[34] Lei H, Hu R, Choi E S, Warren J B and Petrovic C 2010 *Phys. Rev. B* **81** 094518